

Conductivity prediction model for ionic liquids using machine learning

Cite as: J. Chem. Phys. 156, 214505 (2022); doi: 10.1063/5.0089568

Submitted: 26 February 2022 • Accepted: 12 May 2022 •

Published Online: 7 June 2022



R. Datta,¹ , R. Ramprasad,² and S. Venkatram^{2,a)}

AFFILIATIONS

¹The Galloway School, Atlanta, Georgia 30327, USA

²The School of Materials Science and Engineering, Georgia Institute of Technology, Atlanta, Georgia 30332, USA

Note: This paper is part of the JCP Special Topic on Chemical Design by Artificial Intelligence.

a) Author to whom correspondence should be addressed: shruti.v93@gmail.com

ABSTRACT

Ionic liquids (ILs) are salts, composed of asymmetric cations and anions, typically existing as liquids at ambient temperatures. They have found widespread applications in energy storage devices, dye-sensitized solar cells, and sensors because of their high ionic conductivity and inherent thermal stability. However, measuring the conductivity of ILs by physical methods is time-consuming and expensive, whereas the use of computational screening and testing methods can be rapid and effective. In this study, we used experimentally measured and published data to construct a deep neural network capable of making rapid and accurate predictions of the conductivity of ILs. The neural network is trained on 406 unique and chemically diverse ILs. This model is one of the most chemically diverse conductivity prediction models to date and improves on previous studies that are constrained by the availability of data, the environmental conditions, or the IL base. Feature engineering techniques were employed to identify key chemo-structural characteristics that correlate positively or negatively with the ionic conductivity. These features are capable of being used as guidelines to design and synthesize new highly conductive ILs. This work shows the potential for machine-learning models to accelerate the rate of identification and testing of tailored, high-conductivity ILs.

Published under an exclusive license by AIP Publishing. <https://doi.org/10.1063/5.0089568>

I. INTRODUCTION

Since 1986, the number of publications and patents related to ionic liquids (ILs) has grown exponentially due to their potential use in applications ranging from batteries, supercapacitors, and fuel cells, to dye-sensitized solar cells and sensors.^{1–9} These devices currently utilize traditional molecular liquids (such as inorganic dyes, organic liquid solvents, and alkyl carbonates), which have the drawbacks of being volatile, flammable, expensive, or limited in their conductivity and efficiency.^{10–15}

ILs are salts that exist as liquids at ambient temperatures because of their low melting points (up to ~ 373 K¹⁶), which result from the asymmetric cations and anions they are composed of.^{10,15,17} These liquids exhibit high ionic conductivities and high thermal stability, unlike traditional molecular liquids, making them safe and effective candidates for electrolyte replacement in batteries and fuel cells.^{15,18–20} They are already being implemented successfully as electrolytes in rechargeable batteries, fuel cells, and

supercapacitors, as micro-electrodes in biosensors, and as redox mediators in dye-sensitized solar cells.^{11,21–24}

Screening and synthesizing the optimal ILs for these applications, however, is difficult. The current experimental methods to determine the ionic conductivity of ILs are labor-intensive and can require expensive compound-specific equipment and techniques.^{1,11,25} These problems are exacerbated when trying to synthesize tailored ILs with target conductivities.^{26,27} Data-driven methods based on already existing data to determine ionic conductivity can save time and reduce expenditure by eliminating the need to purchase, refine, or synthesize ILs.²⁸ Given the massive number of theoretical ILs (estimated to be up to 10^{18} liquids¹), efficient data-driven methods will allow more research to be conducted on both traditional and customized, application-specific ILs.²⁹

Many prior works predicting the ionic conductivity of ILs are limited by ion-specificity, empirical parameters, or are unable to predict values over a continuous temperature range.^{30–32} While

these models may feature low error metrics, they are based on less comprehensive training data, limited by the environmental conditions (high-temperature or low-temperature environments), or constrained by specific cations (pyridinium, imidazolium, and ammonium).^{33–36} For example, the study of Nilsson-Hallén *et al.*³⁰ predicts ionic conductivity based on only 22 unique ILs within the temperature range of 298.15–368.15 K and requires many experimentally or environmentally determined inputs, such as ion volume and ion mass.

In this work, we build a deep neural network to predict temperature-dependent conductivity values of ionic liquids, trained on experimentally measured and published conductivity data sourced from the ILThermo database.³⁷ Our dataset consists of 406 unique ILs with values over a temperature range from 203.4 to

468.15 K (4259 unique data-points) and ionic conductivities spanning 8 orders of magnitude (3×10^{-7} to 9.795 S/m). The resulting machine learning (ML) model is able to rapidly and accurately predict the ionic conductivity of ILs over a wide range of temperatures. To better understand our ML model, we also investigate and present key chemical features and trends that affect the ionic conductivity in ILs. Our model and associated chemo-structural findings may allow for more efficient screening and designing of new, tailored ILs.³⁸

II. DATASET AND METHODOLOGY

A. Dataset

Our dataset consists of experimentally measured ionic conductivity values of 406 pure compound, binary ionic liquids over

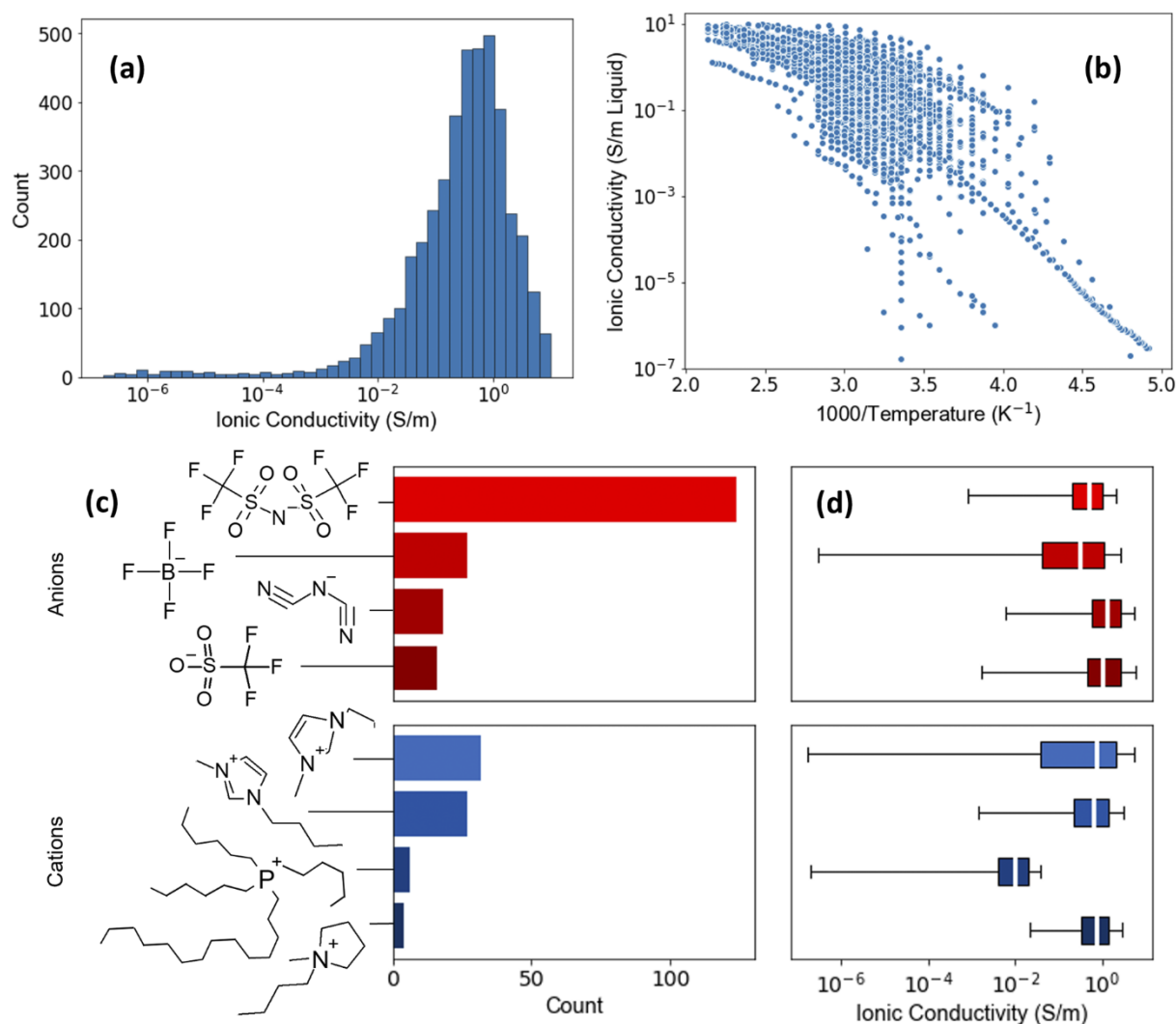


FIG. 1. Experimentally measured dataset for the ionic conductivity of ILs. (a) Histogram for the ionic conductivity of 406 unique ILs at various temperatures. (b) The ionic conductivity vs $1000/\text{temperature}$ relationship for all data-points in the dataset. (c) The most common anions and cations present in the dataset and the number of ILs in which they appear. (d) The median ionic conductivity of ILs featuring the anions and cations of (c) along with their corresponding interquartile range (center 50% of data).

a temperature range from 203.4 to 468.15 K. The data were obtained from the publicly available and peer-reviewed NIST (National Institute of Standards and Technology) ILThermo ionic liquids database.³⁷ We chose to include only two-component (an anion and a cation) pure ILs in our dataset, which features 109 unique anions and 244 unique cations comprised of nine chemical species, including H, B, C, N, O, F, P, S, and I. The most frequently appearing anions were bis((trifluoromethyl)sulfonyl)amide and tetrafluoroborate, appearing in 124 and 27 unique liquids, respectively. The most frequently occurring cations were 1-ethyl-3-methylimidazolium and 1-butyl-3-methylimidazolium, appearing in 32 and 27 unique ILs, respectively. The four most frequently occurring cations and anions are depicted in Fig. 1(c) along with their count. The pressure at which the conductivity for all ILs was measured remains at roughly atmospheric pressure. The complete dataset is attached in the [supplementary material](#).

As shown in Fig. 1(a), conductivity values range from 3×10^{-7} to 9.795 S/m. The majority of the data lie between 10^{-1} and 10^0 S/m. Data are sparse for conductivity values lower than 10^{-2} S/m. In order to account for the data spanning multiple orders of magnitude, we converted the conductivity values into the logarithmic (base 10) scale so each data-point had equal weight in training, validation, and testing.

Figure 1(b) shows the conductivity distribution of the dataset as a function of 1000/temperature. Higher temperature leads to increased ion mobility, leading to greater ionic conductivity values.³⁹ This temperature-based conductivity of ionic liquids can be accurately modeled by Vogel–Tamman–Fulcher (VTF) type equations.⁴⁰ The data show a positive correlation between the temperature of the ILs and their ionic conductivity. When predicting with the ML model over a given temperature range, it is important that the predicted values follow a similar pattern.

In cases where multiple conductivity values were reported for the same IL under the same temperature, the median values were computed and used to reduce dataset uncertainty and achieve lower model error metrics. The median has been shown to be a more robust estimator of the central data point than the mean and is also more resistant to outlier values and skewed data distributions.^{41,42}

B. Featurization

The next step in making an accurate predictive model is to generate features that uniquely represent each IL while also capturing its temperature dependency. The features are derived from the IL's SMILES (simplified molecular-input line-entry system) string. To achieve this, we used the Rdkit.Chem⁴³ python library to generate 163 structural descriptors for each IL, including 2D fragment descriptors and MQNs (molecular quantum numbers). Fragment descriptors are easily computable counts of repeating structural features on a two-dimensional representation of the molecule. MQNs are structural descriptions of the atom, bond, and ring types present within the molecules.⁴⁴ In addition, the temperature at which the ionic conductivity was measured is incorporated as the key feature to encode the temperature dependence, resulting in a 164-dimensional feature vector. In training, all feature values were normalized from 0 to 1.

We used the Least Absolute Shrinkage and Selection Operator (LASSO) reduction method to identify the most important

features.⁴⁵ This method was used to fit the entire dataset (406 ILs) and its original 164 features.

C. Machine learning model and training procedures

Considering that the conductivity depends on both the IL composition and the temperature, the ML model was trained in two distinct fashions. The two approaches are referred to as the (1) IL-split (406 ILs) and (2) data-points-split (4258 points) method. In the IL-split approach, the test data are comprised of entirely unique ILs, resulting in an assessment of the model's performance on ILs with an unseen chemical structure. In the data-points-split approach, random sampling was used to create the train-validation-test sets across a wider range of ILs and temperatures to test how well the model predicts temperature dependency.

Both the IL-split and data-points-split methods utilize the same deep neural network architecture, which was manually tuned. Built with PyTorch,⁴⁶ the ML model has a five-layer architecture (three hidden layers), 160 neurons in each layer, and they back-propagate using the Mean Squared Error (MSE) loss function and Adam optimization.⁴⁷ While this architecture may seem inordinate for our dataset, it proved to be the most efficient and accurate: testing results can be seen in Fig. S1 in the [supplementary material](#). The Adam optimizer tuned the model's hyper-parameters, such as the learning rate and neuron weight to ensure that we had the most efficient and effective model. Both training methods utilized the same train-validation-test splits, each of 80% training data, 10% validation data, and 10% test data. Two error metrics, root mean squared error (RMSE) and the coefficient of determination (R^2), were used to gauge the performance of the model.

Learning curves were also used to measure the performance of the two training methods. The average training and test RMSE is graphed as a function of the training set size, which grows in increments of 10% while the test set remained constant. The error bars represent one standard deviation in the RMSE values over 5 runs.

III. RESULTS AND DISCUSSION

A. Model performance and validation

Figure 2 shows the results of the deep neural network trained with the IL-split method and the data-points-split method. Figures 2(a-i) and 2(b-i) show the learning curves of the machine learning (ML) model trained with the two methods. Results for both the model with all 164 features (ML- X_{ALL}) and the model with the 23 LASSO reduced features (ML- X_{LASSO}) are included. Figures 2(a-ii) and 2(b-ii) show the parity plots (the experimentally measured ionic conductivity is plotted against the predicted ionic conductivity) for the test data using both training methods. Figures 2(a-iii) and (b-iii) show the experimental and ML predicted conductivity values plotted against 1000/temperature for three unique ILs using the IL-split method and the data-points-split method, respectively.

Figure S2 in the [supplementary material](#) is a table with the error values of the ML predictions classified at different levels of conductivity using both training methods.⁴⁸

In both Figs. 2(a-i) and 2(b-i), the test RMSE decreased as the amount of training data increased, as anticipated. We also note

(a) IL-split

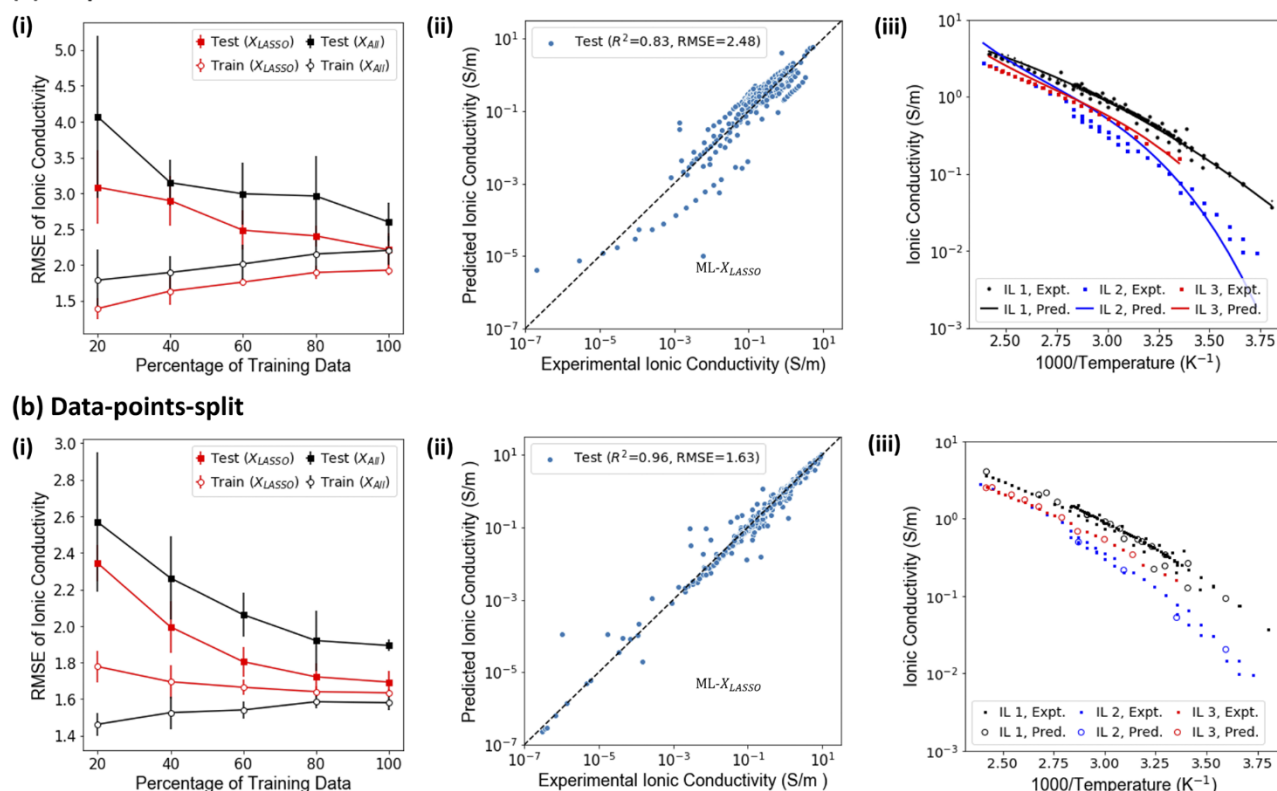


FIG. 2. Performance of ML model predicting ionic conductivity based on IL-split (a) and data-points-split (b) training methods. (a-i) and (b-i) Learning curves trained using all features (ML-X_{ALL}) and LASSO reduced features (ML-X_{LASSO}). (a-ii) and (b-ii) Parity plots using ML-X_{LASSO} and the 80% train set. (a-iii) and (b-iii) The experimental and ML predicted conductivity values for three unique ILs. IL 1 is 1-butyl-1-methylpyrrolidinium bis(trifluoromethyl)sulfonylimide, IL 2 is 1-methyl-3-octylimidazolium tetrafluoroborate, and IL 3 is 1-hexyl-1-methylpyrrolidinium bis(trifluoromethanesulfonyl)imide.

that the ML-X_{LASSO} model outperforms the ML-X_{ALL} model in regard to test RMSE. With the data-points-split method, we obtain a test RMSE of 1.69 and 1.89, and with the IL-split method; a test RMSE of 2.21 and 2.60 using the ML-X_{LASSO} and ML-X_{ALL} models, respectively.

In addition, the learning curves show a systemic gap between the training and test curves with the train curves having consistently lower errors that are demonstrative of a model that is not over-fitted. We observe that the test RMSE values for the data-points-split method are consistently lower than that of the IL-split method. This trend is to be expected since the data-points-split method is a less arduous ML task. For a given IL, the data-points-split method provides partial data points at a given temperature in addition to the chemical fingerprints; however, for the IL-split method, the only input provided to a model is the chemical fingerprints of the IL and the model is expected to extrapolate using other discrete ILs with similar features to predict temperature-dependent IL conductivities. To present the model's error in context, we calculated the Normalized RMSE (NRMSE).⁴⁹ Considering our dataset ranges from 3×10^{-7} to 9.795 S/m, we calculated a percent NRMSE of 22.5%. This error value is appropriate

given the large scope of the model's dataset and, therefore, target applications.

The R² values for the test set of the IL-split and data-point-split methods [shown in Figs. 2(a-ii) and 2(b-ii), respectively] are 0.88 and 0.97, respectively. Because the training data are sparse below 10^{-3} , it can be seen that the predictions at that level are less accurate than those at higher values.

In Fig. 2(a-iii), the lines of best fit were applied to the discrete ML predicted values to more clearly show the conductivity under which the model predicts less accurately. In all three example ILs, the model under-predicts conductivity at extremely low temperatures and slightly over-predicts at high temperatures. This is likely because of the sparse training data at temperatures under 285 K.

In Fig. 2(b-iii), the experimentally determined values (found in the training dataset) were plotted alongside predicted values (not found in training or validation) of the same three ILs.

Overall, Fig. 2 shows that the data-points-split-based ML model performed better than the IL-split-based model, as seen in the RMSE, R², and learning curve error trends. This is expected, given that the data-points-split training dataset includes a wider variety of IL species, features, and chemical compositions. It is possible

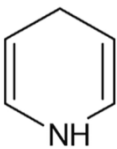
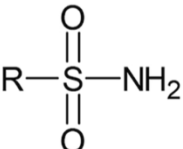
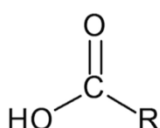
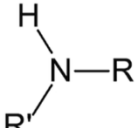
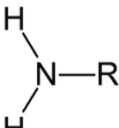
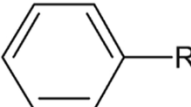
Correlation with ionic conductivity	Representative features		
Positive correlation	$R-X$	$R-C\equiv N$	
			
Number of acyclic Nitrogen atoms, number of acyclic double and triple bonds, number of H-bond acceptor sites and atoms, number of positive charges			
Negative correlation			
	$R-OH$	$Ar-CH_3$	
	Number of unbranched alkanes (of at least 4 members), number of aromatic carbocycles, number of Bromine and Phosphorus atoms		

FIG. 3. LASSO selected features with strong positive or negative correlations with the ionic conductivity. R represents an arbitrary alkane. Ar represents an arbitrary aromatic group. X represents an arbitrary Halogen group.

that, in the data-points-split approach, many of the same ILs were included in training and testing at different temperatures, improving the results. Theoretically, the data-points-split-based model could be used to make predictions on ILs with some already known temperature-based conductivity values, while the IL-split-based model could be used on completely new ILs, with no available conductivity data.

B. Guidelines to design high conductivity ionic liquids

While most ILs in sparse regions of the dataset were well predicted, a few ILs that were severely under-predicted had low acyclic nitrogen and H-bond acceptor site counts. The LASSO reduced features offer insight into the factors that affect ionic conductivity. Figure 3 lists some of the features that have strong correlations with ionic conductivity. All 22 LASSO reduced features and their

respective correlation with the ionic conductivity can be seen in Fig. S3 in the [supplementary material](#). Positive and negative coefficients resulting from LASSO reduction correspond to positive and negative correlations with ionic conductivity, respectively.

It is important to note that the number of nitriles, primary sulfonamides, halogen bonds, H-bond acceptor sites and atoms, positive charges, and acyclic double and triple bonds correlate positively with the ionic conductivity. This is likely because of the increased polarity, degree of ionization, ion pairing, charge density, and reduction of the LUMO–HOMO gap of the liquid.^{50–53} Unsaturated carbon–carbon bonds and the resulting pi orbitals present within these features contribute to the positive correlation with conductivity due to the increased polarizability and charge delocalization.^{54,55} When negatively charged ions, such as aliphatic carboxylic acids and aliphatic hydroxyl groups, and non-conductive groups like unbranched alkanes (of four or more members) are introduced, the

conductivity is reduced. These long aliphatic side chains decrease conductivity as a result of the increased viscosity of the ILs.^{9,48,56} Aromatic groups, such as aryl methyl sites and benzene rings, also had a negative correlation with the ionic conductivity, likely because of the resultant pi stacking.^{57,58}

This information can be used to create a framework to help accelerate the synthesis of ILs with ionic conductivity customization as the target. Given the goal of high ionic conductivity, liquids should be synthesized with characteristics that increase the ion charge density of the liquid, such as double and triple bonds and hydrogen bond acceptors. Alternatively, to control or reduce the ionic conductivity, negatively charged ions and aromatic groups could be targeted. Combining these guidelines with instantaneous predictions from the neural network can allow new compounds to be rapidly synthesized and tested.

IV. CONCLUSION

We have developed a machine learning (ML) model capable of making instantaneous ionic conductivity predictions for ionic liquids (ILs). We have also constructed a set of guidelines for the design and synthesis of new ILs. This model is trained using a dataset of experimentally measured ionic conductivity values for 406 unique ILs featurized into structural and fragment descriptors, MQNs, and temperature. The performance of the model was tested with 40 unseen ILs or 3406 data-points and has proven to be more comprehensive in its predictions than previous works using ML models to predict the ionic conductivity of ILs. Furthermore, our model does not require many calculated or physically obtained inputs; it simply uses the SMILES string and target temperature(s). Unique ILs with low ionic conductivities (<0.1 S/m) may have a larger margin of error. These data along with data at lower temperature values could be added to the training dataset to further improve the model manually or through active learning.

We identified important chemo-structural features that correlated positively or negatively with the ionic conductivity, which can be used to design new ILs with tailored ionic conductivity values. Subsequently, the ML model can quickly and accurately assess the conductivity of these newly designed ILs. It is important to note that the conductivity is only one material property that must be taken into consideration before implementing ILs. For example, the viscosity and density of ILs are key to their implementation in energy applications along with conductivity. Future works may include multi-output regression models to integrate multiple key properties, aggregating multiple IL databases. It is also important to note that the presented ML model is trained on pure-compound ILs; future models could be constructed for binary or ternary mixtures. By increasing the efficiency of design, synthesis, and testing, we anticipate that this approach may have a major impact on the future development and applications of tailored ionic liquids.

SUPPLEMENTARY MATERIAL

See the [supplementary material](#) for Figs. S1–S3.

AUTHOR DECLARATIONS

Conflict of Interest

The authors have no conflicts to disclose.

DATA AVAILABILITY

The dataset used in this study has been created from the ILThermo Ionic Liquids database. The complete dataset with the LASSO reduced features is attached (Supplementary Dataset).

REFERENCES

1. N. V. Plechkova and K. R. Seddon, *Chem. Soc. Rev.* **37**, 123 (2008).
2. N. Yamanaka, R. Kawano, W. Kubo, T. Kitamura, Y. Wada, M. Watanabe, and S. Yanagida, *Chem. Commun.* **2005**, 740.
3. B. Garcia, S. Lavallée, G. Perron, C. Michot, and M. Armand, *Electrochim. Acta* **49**, 4583 (2004).
4. E. G. Yanes, S. R. Gratz, M. J. Baldwin, S. E. Robison, and A. M. Stalcup, *Anal. Chem.* **73**, 3838 (2001).
5. C. A. Zell and W. Freyland, *Langmuir* **19**, 7445 (2003).
6. C. W. Scheeren, G. Machado, J. Dupont, P. F. P. Fichtner, and S. R. Teixeira, *Inorg. Chem.* **42**, 4738 (2003).
7. L. He, W. Zhang, L. Zhao, X. Liu, and S. Jiang, *J. Chromatogr. A* **1007**, 39 (2003).
8. Y. Zhou and M. Antonietti, *J. Am. Chem. Soc.* **125**, 14960 (2003).
9. A. B. McEwen, H. L. Ngo, K. LeCompte, and J. L. Goldman, *J. Electrochem. Soc.* **146**, 1687 (1999).
10. M. A. Navarra, *MRS Bull.* **38**, 548 (2013).
11. H. Ohno, *Electrochemical Aspects of Ionic Liquids* (John Wiley & Sons, 2005), pp. 1–3.
12. Z. Yang and W. Pan, *Enzyme Microb. Technol.* **37**, 19 (2005).
13. K. Sharma, V. Sharma, and S. S. Sharma, *Nanoscale Res. Lett.* **13**(1), 381 (2018).
14. L. Gaines and R. Cuenca, *Technical Report*, Center for Transportation Research Argonne National Laboratory, 2000.
15. C. Arbizzani, G. Gabrielli, and M. Mastragostino, *J. Power Sources* **196**, 4801 (2011).
16. R. D. Rogers, *ACS Symposium Series* (American Chemical Society, 2002).
17. W. H. Meyer, *Adv. Mater.* **10**, 439 (1998).
18. D. R. MacFarlane, N. Tachikawa, M. Forsyth, J. M. Pringle, P. C. Howlett, G. D. Elliott, J. H. Davis, M. Watanabe, P. Simon, and C. A. Angell, *Energy Environ. Sci.* **7**, 232 (2014).
19. R. F. De Souza, J. C. Padilha, R. S. Gonçalves, and J. Dupont, *Electrochem. Commun.* **5**, 728 (2003).
20. M. J. Earle and K. R. Seddon, *Pure Appl. Chem.* **72**, 1391 (2000).
21. M.-C. Lin, M. Gong, B. Lu, Y. Wu, D.-Y. Wang, M. Guan, M. Angell, C. Chen, J. Yang, B.-J. Hwang *et al.*, *Nature* **520**, 324 (2015).
22. A. Eftekhari, *Energy Storage Mater.* **9**, 47 (2017).
23. S. Denizalti, A. K. Ali, Ç. Ela, M. Ekmekci, and S. Erten-Ela, *Chem. Phys. Lett.* **691**, 373 (2018).
24. D. Wei and A. Ivaska, *Anal. Chim. Acta* **607**, 126 (2008).
25. A. K. Burrell, R. E. Del Sesto, S. N. Baker, T. M. McCleskey, and G. A. Baker, *Green Chem.* **9**, 449 (2007).
26. S. K. Singh and A. W. Savoy, *J. Mol. Liq.* **297**, 112038 (2020).
27. R. Ratti, *Adv. Chem.* **2014**, 729842.
28. R. Ramprasad, R. Batra, G. Pilania, A. Mannodi-Kanakkithodi, and C. Kim, *npj Comput. Mater.* **3**, 54 (2017).
29. G. Pilania, A. Mannodi-Kanakkithodi, B. Uberuaga, R. Ramprasad, J. Gubernatis, and T. Lookman, *Sci. Rep.* **6**, 19375 (2016).
30. J. Nilsson-Hallén, B. Ahlström, M. Marczewski, and P. Johansson, *Front. Chem.* **7**, 126 (2019).
31. Z. K. Koi, W. Z. N. Yahya, and K. A. Kurnia, *New J. Chem.* **45**, 18584 (2021).

- ³²I. Baskin, A. Epshtein, and Y. Ein-Eli, *J. Mol. Liq.* **351**, 118616 (2022).
- ³³A. P. Abbott, *ChemPhysChem* **6**, 2502 (2005).
- ³⁴E. Kianfar, M. Shirshahi, F. Kianfar, and F. Kianfar, *Silicon* **10**, 2617 (2018).
- ³⁵D. V. Duong, H.-V. Tran, S. K. Pathirannahalage, S. J. Brown, M. Hassett, D. Yalcin, N. Meftahi, A. Christofferson, T. L. Greaves, and T. C. Le, *J. Chem. Phys.* **156**, 154503 (2022).
- ³⁶P. Dhakal and J. K. Shah, *Fluid Phase Equilib.* **549**, 113208 (2021).
- ³⁷A. Kazakov, J. Magee, R. Chirico, V. Diky, K. Kroenlein, C. Muzny, and M. Frenkel, *Ionic liquids database–ilthermo (v2.0)*, 2013.
- ³⁸R. Batra, L. Song, and R. Ramprasad, *Nat. Rev. Mater.* **6**, 655 (2021).
- ³⁹J. J. Barron and C. Ashton, TSP report, 2005.
- ⁴⁰J. Vila, P. Ginés, J. M. Pico, C. Franjo, E. Jiménez, L. M. Varela, and O. Cabeza, *Fluid Phase Equilib.* **242**, 141 (2006).
- ⁴¹A. Jha, A. Chandrasekaran, C. Kim, and R. Ramprasad, *Modell. Simul. Mater. Sci. Eng.* **27**, 024002 (2019).
- ⁴²M. Pagano and K. Gauvreau, *Principles of Biostatistics* (CRC Press, 2018).
- ⁴³G. Landrum, RDKit: Open-Source Cheminformatics Software, Q2 (2006); available at <https://www.rdkit.org/>.
- ⁴⁴K. T. Nguyen, L. C. Blum, R. Van Deursen, and J.-L. Reymond, *ChemMedChem* **4**, 1803 (2009).
- ⁴⁵F. Pedregosa, G. Varoquaux, A. Gramfort, V. Michel, B. Thirion, O. Grisel, M. Blondel, P. Prettenhofer, R. Weiss, V. Dubourg, J. Vanderplas, A. Passos, D. Cournapeau, M. Brucher, M. Perrot, and E. Duchesnay, *J. Mach. Learn. Res.* **12**, 2825 (2011).
- ⁴⁶A. Paszke, S. Gross, F. Massa, A. Lerer, J. Bradbury, G. Chanan, T. Killeen, Z. Lin, N. Gimelshein, L. Antiga, A. Desmaison, A. Kopf, E. Yang, Z. DeVito, M. Raison, A. Tejani, S. Chilamkurthy, B. Steiner, L. Fang, J. Bai, and S. Chintala, *Advances in Neural Information Processing Systems* (Curran Associates, Inc., 2019), Vol. 32, pp. 8024–8035.
- ⁴⁷D. P. Kingma and J. Ba, *arXiv:1412.6980* (2014).
- ⁴⁸M. Galiński, A. Lewandowski, and I. Stępnia, *Electrochim. Acta* **51**, 5567 (2006).
- ⁴⁹M. V. Shcherbakov, A. Brebels, N. L. Shcherbakova, A. P. Tyukov, T. A. Janovsky, V. A. Kamaev *et al.*, *World Appl. Sci. J.* **24**, 171 (2013).
- ⁵⁰Y. Kubota and Y. Tominaga, *Mater. Today Commun.* **4**, 124 (2015).
- ⁵¹V. Morizur, S. Olivero, J. R. Desmurs, P. Knauth, and E. Duñach, *New J. Chem.* **38**, 6193 (2014).
- ⁵²M. H. Matus, J. Garza, and M. Galván, *J. Phys. Chem. B* **110**, 1172 (2006).
- ⁵³T. Mukai and K. Nishikawa, *RSC Adv.* **3**, 19952 (2013).
- ⁵⁴K. Tsunashima, Y. Ono, and M. Sugiya, *Electrochim. Acta* **56**, 4351 (2011).
- ⁵⁵C. D. Rodríguez-Fernández, E. L. Lago, C. Schröder, and L. M. Varela, *J. Mol. Liq.* **346**, 117099 (2022).
- ⁵⁶M. Montanino, M. Carewska, F. Alessandrini, S. Passerini, and G. B. Appetecchi, *Electrochim. Acta* **57**, 153 (2011).
- ⁵⁷S. T. Schneebeli, M. Kamenetska, Z. Cheng, R. Skouta, R. A. Friesner, L. Venkataraman, and R. Breslow, *J. Am. Chem. Soc.* **133**, 2136 (2011).
- ⁵⁸M. Alsufyani, R. K. Hallani, S. Wang, M. Xiao, X. Ji, B. D. Paulsen, K. Xu, H. Bristow, H. Chen, X. Chen *et al.*, *J. Mater. Chem. C* **8**, 15150 (2020).